UCRL-84235
PREPRINT
CONF-801011--6

THE TECHNOLOGY OF DIRECT CONVERSION FOR MIRROR REACTOR END-LOSS PLASMA

MASTER

W. L. Barr
R. W. Moir

This paper was prepared for submittal to

Fourth ANS Topical Meeting on the Technology of Controlled Nuclear Fusion

King of Prussia, Pennsylvania
October 14-17, 1980

October 7, 1980

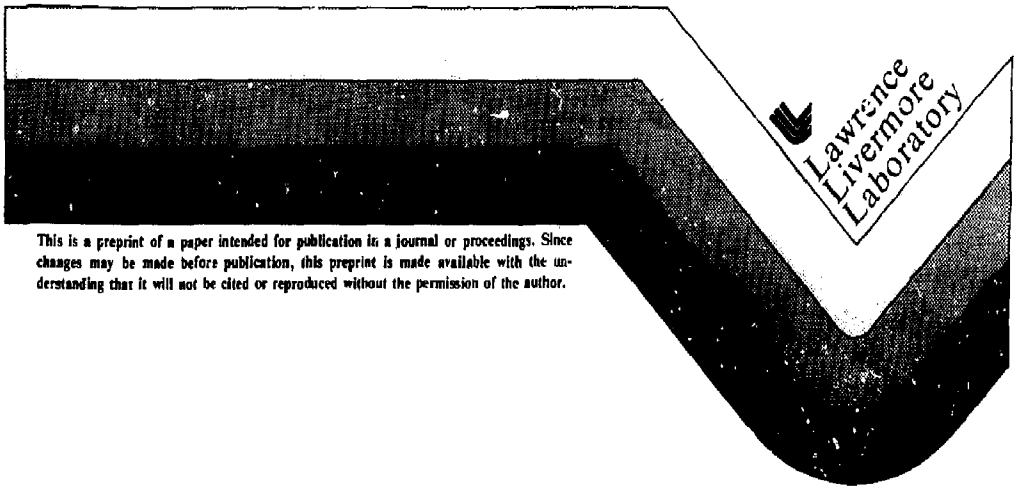

THE TECHNOLOGY OF DIRECT CONVERSION FOR MIRROR REACTOR END-LOSS PLASMA*

W. L. Barr and R. W. Moir
Lawrence Livermore National Laboratory, University of California
Livermore, California, USA 94550

Summary

Design concepts are presented for plasma direct convertors (PDC) intended primarily for use on the end-loss plasma from tandem-mirror reactors. Recent experimental results confirm most of these design concepts. Both a one-stage and a two-stage PDC were tested in reactor-like conditions using a 100-kV, 6-kW ion beam. In a separate test on the end of the TMX machine, a single stage PDC recovered 79 W for a net efficiency of 50%. Tandem mirror devices are well suited to PDC. The high minimum energy of the end-loss ions, the magnetic expansion outside the mirrors, and the vacuum conditions in the end tanks required by the confined plasma, all preexist. The inclusion of a PDC is therefore a rather small addition. These facts and the scale parameters for a PDC are discussed.

Introduction

The results from two recent plasma direct conversion (PDC) experiments support the design concepts for PDC's that are being used in mirror fusion reactor studies. One experimental test was done in reactor-like conditions[1] (100 keV, 10^{-5} Torr, 75 W/cm^2) and one was done at lower power and energy (1 keV, 1 W/cm^2) on the end-loss plasma in the TMX machine.[2] In both cases the results agreed with predictions. The unit tested on TMX had only a single collector stage, while both a single-stage and a two-stage PDC was tested on the high-power test stand.

A single stage PDC (see Fig. 1) consists of two highly transparent grids followed by a solid collector plate. The entrance grid is usually held at ground potential, while the repeller grid is held negative to prevent electrons from reaching the positive collector plate. The collector plate receives a net positive current which is used to drive a load. Collector voltage is developed across the load and is controlled by adjusting the resistance of the load. When

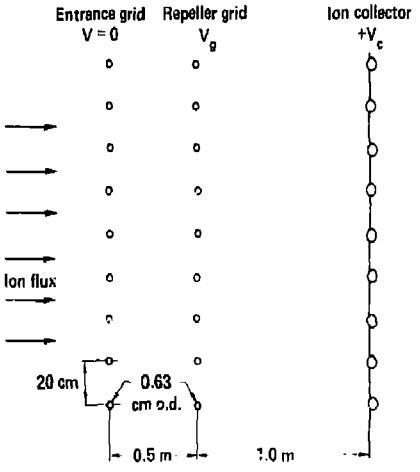

Fig. 1. A single-stage plasma direct converter with a grounded grid, an electron suppressor grid, and an ion collector.

the collector voltage is raised, the collector current decreases because fewer ions are able to reach the collector. The optimal load resistance is the one that results in the most power (current × voltage product) at the load, and it depends on the energy distribution of the ions arriving at the PDC.

A two-stage PDC can recover more power because the intermediate collector stage recovers most of those ions that are turned back by the higher potential of the second collector. Figure 2 shows a sketch of a two-stage, Venetian-blind PDC. The ions arrive at a small angle from the normal so that any reflected ions follow curved trajectories. The Venetian-blind structure is designed to intercept few incident ions, but all of the reflected ions. Another suppressor grid follows the intermediate stage to prevent the secondary electrons produced on the first stage from flowing to the second stage.

*Work performed under the auspices of the U. S. Department of Energy by the Lawrence Livermore National Laboratory under contract number W-7405-ENG-48.

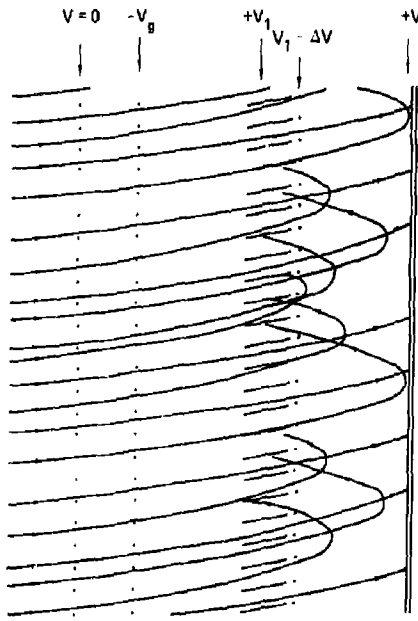

Fig. 2. A two-stage plasma direct converter of the Venetian-blind type. The intermediate collector receives those ions that are turned back before reaching the second collector at higher potential.

The potentials of the two collectors are chosen to produce the maximum output power. These optimal values depend on the energy distribution of the ions entering the PDC.

The energy distribution of the end-loss ions in a mirror machine is ideally suited for energy recovery because of the high mean energy, and especially because of the high minimum energy. Tandem-mirror machines have high minimum energies because of the high plasma potential in the end plugs which serve to stopper the end loss of ions from the central cell. Also, the two origins of end-loss ions (central cell and plugs) results in two energy groups which suggest a two-stage PDC.

In mirror machines, some of the injected power and fuel is consumed in producing fusion power, but most is lost out the ends. This is true in tandem-mirror machines as well, although the loss is less in a tandem because of the higher Q. The fraction of injected fuel that is burned is directly proportional to $Q \equiv P_F/P_{in}$, where P_F is the fusion power produced and P_{in} is the power that is consumed in heating and fueling the plasma. Since two fuel ions are used to produce one fusion reaction, the rate I_b that fuel ions are consumed is $I_b = 2P_F/E_F$, where E_F is the energy produced in each fusion reaction. Expressing P_F in terms of Q and setting $P_{in} = I_{in}E_{in}$, with E_{in} equal to the total heating power divided by the fuel current, gives $I_b/I_{in} = 2QE_{in}/E_F$. Typically, $E_{in}/E_F \sim 0.01$ so that a $I_b/I_{in} \sim 2Q$ percent. Therefore, the power lost out the ends of a tandem in the form of kinetic energy of escaping fuel is typically 80% of the heating power. In a high-Q machine this may be an acceptable loss (being only ~8% of P_F), but even there it is as important to recover this power as it is to improve the efficiency of the plasma heating system.

Particle Currents and Energies at the Direct Converter

In the tandem mirror concept,[3,4] the positive plasma potential of a standard mirror machine at each end is used to plug the loss of plasma from a long central solenoid. Figure 3 shows a sketch of the potential and the magnetic field in a simple tandem mirror configuration. Recent modifications of this configuration[5] (i.e., the addition of barrier cells) affect the electrons but don't change the ion energy distribution at the ends, which is the point of interest here.

On the average each fuel ion that escapes from the center cell has a mean energy of T_{ic} (i.e, central-cell thermal energy in two degrees of freedom), and is then accelerated by the potential difference $\phi_c + \phi_e$ before reaching the PDC (See Fig. 2). The average ion energy is

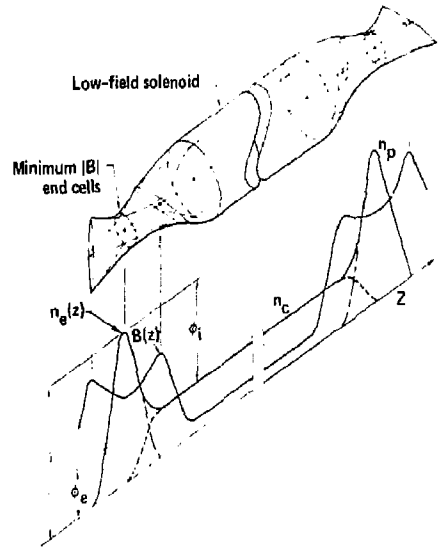

Fig. 3. Tandem mirrors with ambipolar barriers at the ends.

therefore $T_{ic} + e(\phi_c + \phi_e)$ at the PDC, and the minimum energy is $e(\phi_c + \phi_e)$. Ideally, a PDC with collector potential equal to $\phi_c + \phi_e$ could recover all the escaping central-cell ions with an average excess energy of T_{ic}. The excess energy would appear as heat. Typically T_{ic} is small in comparison with $e(\phi_c + \phi_e)$, so the efficiency of direct recovery would be high. The many loss mechanisms discussed here degrade this ideal efficiency to a somewhat lower value.

The current, I_c, of lost fuel ions from the central cell is equal to the total number confined at one time divided by the mean confinement time, τ_c. That is,

$$I_c = en_c^2 V_c/(n\tau)_c \quad ,$$

where n_c is the density and V_c the volume of the central-cell plasma.

The plugs are standard, minimum B, mirror machines whose purpose is to provide the high ambipolar potential to stopper (plug) the ends of the central cell. To be confined in a plug, an ion's velocity vector must lie outside the loss cone defined by the magnetic mirror ratio, R_p, and the plug potential, $\phi_c + \phi_e$. The minimum kinetic energy that an ion can have and still be confined in a plug is $e(\phi_c + \phi_e)/(R_p-1)$, and after acceleration by the potential difference this minimum-energy ion could arrive at the PDC with an energy of $R_p e(\phi_c + \phi_e)/(R_p-1)$. On the average, plug ions arrive at the PDC with T_{ip} more than this minimum energy, where T_{ip} is the ion temperature in the plugs. The current of ions from both plugs to the PDC is

$$I_p = 2en_p^2 V_p/(n\tau)_p \quad ,$$

by arguments similar to those for I_c.

In one recent study[6], I_c = 330 A, T_{ic} = 40 keV, $\phi_c + \phi_e$ = 355 kV, I_p = 5A, T_{ip} = 400 keV, and R_p = 1.5. In that case both the current and power from plug ions was almost negligible. The n values needed to evaluate the currents were determined by numerical calculations, but analytic expressions have been developed[7] to estimate them.

In steady state the net negative electron current leaving the plasma must exactly equal the total ion current. Only those electrons in the tail of the energy distribution are able to escape from the positive plasma potential. To the extent that the confined electrons have a Maxwellian energy distribution with a temperature T_e, the loss electrons arrive at the PDC with an average energy of T_e and with zero minimum energy.

The fusion reactions in the central cell produce alpha particles which finally arrive in the end tanks in one of three different energy groups. Because their initial energy is greater than the confining potentials, those alphas that are born within the magnetic loss cone escape immediately with their full 3.52 MeV of energy. Half go out each end and arrive at the PDC with 3.52 MeV + $2e\phi_e$, since the potential difference between central cell and end wall is ϕ_e. The fraction f that are born within the loss cone is

$$f = 1 - \left(\frac{R_{ef} - 1}{R_{ef}}\right)^{1/2} \quad ,$$

where R_{ef} is the effective mirror ratio at the central cell, including the plasma diamagnetic effect. The remaining 1 - f of the alphas are trapped and cooled by the plasma. Some of these are scattered into the loss cone and lost, half out each end, before their kinetic energy is reduced below $2e\phi_c$, where they become electrostatically trapped. The fraction of the alphas that escape in this way and their mean energy when they escape can be calculated numerically. They are accelerated by $2e\phi_e$ before reaching the PDC. The remaining alphas thermalize with the central-cell plasma and eventually diffuse radially to the outer layer near the wall. The magnetic field lines through this outer, annular region are left unstoppered to allow an escape route for the alphas and for cold impurity ions born near the walls. Skimmers backed with cryopanels in the end tanks remove this cold plasma from the outer field lines before it can reach the PDC.

Except for the energetic alphas, the ion-energy distribution at the ends of a tandem mirror reactor is well suited for direct recovery. The distribution tends to be narrow with a high minimum energy--ideal for a single stage PDC. If the power in the end ions from the plugs is significant, a two-stage, Venetian-blind PDC may be more cost effective than a single stage unit.

Power Density at the Direct Converter

The end-loss plasma is guided by the magnetic field in the end tanks. It is restricted to the magnetic flux tube that maps back to the central-cell plasma. For this reason, the cross-sectional area of the end-loss column varies inversely with B, the magnetic field strength, which can therefore be used to control the power density at the PDC. It is necessary to expand the plasma column to reduce the power density from the many kW/cm^2 at the mirrors to a level ($\sim$100 W/cm^2) that can be tolerated by the grids in the PDC.

Expansion serves the equally important purpose of transforming particle motion that is perpendicular to the field lines into motion along the field lines. If the expansion is gradual enough the magnetic moment $\mu = W_\perp/B$ of a charged particle is an approximate constant of the motion. Then, the perpendicular energy, $W_\perp$, must decrease proportionately with B. Numerical

trajectory calculations[8] have shown that is preserved if the variation of B satisfies the inequality,

$$\frac{dB}{dx} < \frac{3B}{p} ,$$

where the pitch length $p = 2\pi Mv_{\parallel}/eB$ is the distance the particle would move along the field line in one gyro period at that value of B. This condition on dB/dx is only approximate, since it can be shown that μ is preserved regardless of dB/dx if the field lines radiate out from a point and are straight.[9] When μ is preserved, the conservation of energy ensures that the decrease in $W_{\perp}$ as B decreases will appear as an equal increase in $W_{\parallel}$, the energy of parallel motion;

$$W_{\parallel} = W(1 - 1/R) ,$$

where $W_{\parallel}$ is the parallel energy at th PDC, W is the total energy, and R is the magnetic expansion ratio from mirror to PDC. Since R > 100 is required to reduce the power density, the energy is nearly all converted into recoverable $W_{\parallel}$.

In the magnetic expansion, there is another restriction on any curvature of the field lines. If the radius of curvature of a field line is less than about one pitch length, p, the guiding center for the particle will be unable to follow the field line. Too much curvature will destroy not only the simple scaling of power density with field strength but also will destroy the one-for-one mapping of regions in the central cell onto regions at the end walls. To avoid these problems, any necessary curvature of the field lines should be concentrated near the mirrors where B is high and the pitch lengths are short.

The power carried by the electrons can make the dominant contribution to the heat load on the grids of the PDC, and this heat load determines the choice of the expansion ratio, R. All of the electron power is eventually deposited on the entrance grid through which the electrons are reflected back and forth between the suppressor grid on one side and the magnetic mirror on the other. Only the small intercepted fraction of the ion power goes into heating the grids. The effective power density, q, at the entrance grid is

$$q = q_i + q_e/(1 - T),$$

where q_i and q_e are the power densities of the ions and electrons, respectively, and T is the transparency of the grid. Since T 0.95 for good recover efficiency, q_e can contribute most of the heating to the entrance grid even though $q_e \ll q_i$. Only q_i is incident on the suppressor grid.

The simplest grid structures are ones that use solid wires cooled only by radiation. In steady state operation, each grid wire must radiate away as much power as it receives from the particles it intercepts. For round wires the condition per unit of length is

$$2rq = 2\pi r\sigma\varepsilon T^4,$$

where r is the radius of the wire, q is the effective beam-power density, $\sigma = 5.7 \times 10^{-12}$ W/cm^2 deg^4 is the Stefan-Boltzmann constant, ε is the emissivity of the wire surface, and T is the temperature of the wire. A q = 100 W/cm^2 produces a temperature of about 1900 K when ε = 0.4. Many high-melting-point materials have an evaporation rate at this temperature of less than 10^{-7} gm/cm^2-s and would survive more than a year if the sputtering rate were also low. The typical sputtering rate of about 10^{-2} atoms/ion for 100 keV D^+ on heavy metals would take several years to erode a wire away.

The maximum allowable grid temperature, and hence the maximum q, is set by the thermionic emission of electrons from the grid wires. Thermionic emission is described by the Richardson-Dushman equation

$$j = A_0T^2e^{-\phi/kT},$$

where j is the saturated thermal emission current density in A/cm^2, A_0 is Dushman's constant whose theoretical value is 120 A/cm^2 deg^2, T is the temperature in Kelvins, φ is the work function in eV, and k is Boltzmann's constant ($k = 8.6 \times 10^{-5}$ eV/K). Measured values of A_0 are typically about half the theoretical value[10]. For tungsten φ = 4.5 eV, A_0 = 70 A/cm^2 deg^2 which results in j = 5 10^{-4} A/cm^2 at 1930 K. This is roughly equal to the currrent density of beam ions when q = 100 W/cm^2, so the wires emit about π thermionic electrons for each intercepted ion. The secondary emission of electrons is an additional effect to be discussed later.

Uncertainties in the values of both ε and φ, because of changes in the wire during operation, cause an uncomfortably large uncertainty in the q that can be allowed. Figure 4 shows a plot of j vs q calculated for round wires with several possible combinations of ε and φ. As a general rule, an emission current density of j = q/W can be allowed, where W is the average energy of the incident ions. For tungsten wires ε can range from 0.23 for a smooth surface[10] to 0.4 for an "etched" one[11] at 1900 k. Rhenium with high values of both φ = 5.1 eV and ε ≈ 0.4 would be better than tungsten, while graphite with φ = 4.6 eV and ε ≈ 0.8 would be even better as far as reduced thermionic emission is concerned. Ribbon-shaped wires could possibly increase the allowed power density because of their greater surface area for cooling. However, the differential expansion would tend to twist them and could cause them to intercept more power from the beam than round wires.

Thermionic emission can be avoided if the grid elements are short enough to allow the use

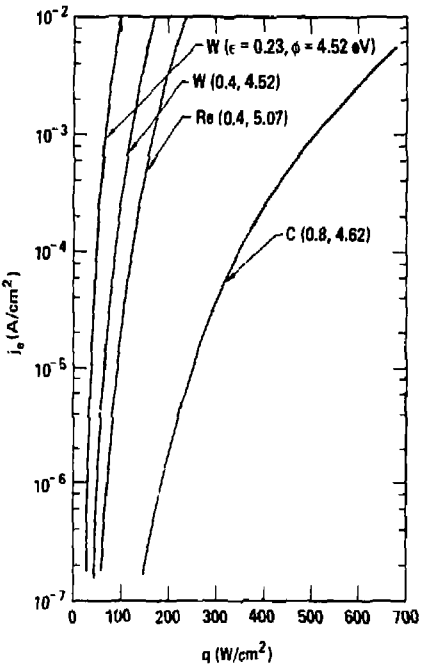

Fig. 4. Thermionic electron emission current vs the power flux on one side of circular grid wires cooled only by radiation.

of convectively cooled hollow tubes instead of wires. When tubes can be used, the power density at the PDC can be increased several fold over the limiting value for wires. It is difficult to establish the power density limit for tubes because of the compromise that must be made between high transparency of the grid and safety against leaks and ruptures. Calculation of the stress in the tube walls[12] is complicated by the differential thermal expansion due to the one-sided heating and central cooling. However, a conservative estimate of the possible power density when the stress on the tubes is not the main issue can be made rather simply.

The steady-state temperature rise T_B of the bulk coolant flowing through a length L of a tube which is being irradiated on one side with power density q is

$$T_B = \frac{q\,L\,d_o}{CQ}$$

where d_o is the outer diameter, C is the heat capacity of the coolant, and Q is the flow rate. The flow depends on several things, including the inside diameter, d_i, of the tube, the pressure gradient, $\Delta p/L$, along the tube, the Reynolds number, and the friction factor, f, for the inside of the tube. For the special case of water flowing in long tubes with $f = 0.03$,

$$Q = 6.4 \times 10^3\, d_i^{5/2}\, (\Delta p/L)^{1/2},$$

where Q is expressed in cm^3/s, d_i and L in cm, and p in atmospheres. Turbulent flow is assumed and requires that $v d_i > 20\ cm^2/s$, where v is the flow velocity. When this Q is combined with the expression for T_B, the result is

$$T_B = \frac{q\,L^{3/2}\,d_o}{2.7 \quad 10^4\, d_i^{5/2}\, \Delta P^{1/2}} ,$$

where we have set $C = 4.18\ J/cm^3$ deg for water.

There is an additional temperature difference, ΔT_{film}, between the bulk cooling water and the inner tube walls. The ΔT_{film} is usually calculated in terms of a heat transfer coefficient which depends mainly on the flow velocity. When the film is not boiling, this transfer coefficient can be expressed in terms of d_i, Δp, and L, giving the temperature difference T_{film} as

$$\Delta T_{film} = 0.080\, q(L^2/\Delta p^2\, d_i)^{1/5}.$$

Actually, q here is not exactly the same as the q incident on the one outer side of the tube. Radial conduction through the tube wall concentrates the heat, and azimuthal conduction spreads it out. We assume here that the two effects cancel.

Finally, there is the temperature difference between inner and outer surfaces of the tube wall on the beam side. To the extent that the radial and azimuthal effects cancel, the conduction through the wall takes place with a constant temperature gradient given simply by

$$\frac{dT}{dx} = \frac{q}{k} ,$$

where k is the thermal conductivity of the tube material. The maximum temperature difference, ΔT_W across the tube wall is therefore

$$\Delta T_W = \frac{q}{k}\, d_o - d_i .$$

Figure 5, supplied by the authors of Ref. 12, shows a sketch of the temperature variation along the length of a tube. The onset of fully developed subcooled nucleate boiling in the outer film occurs at the point labeled ONB. The bulk temperature, T_B, continues to rise beyond ONB until at the point OBB it reaches the value T_{sat} equal to the saturated fluid temperature where bulk boiling occures at the local pressure. For any given length of tube, q must be restricted so that the end of the tube is reached before the point OBB, where burnout is imminent.

The above expression for ΔT_{film} is only accurate up to the point ONB, but we can use it to

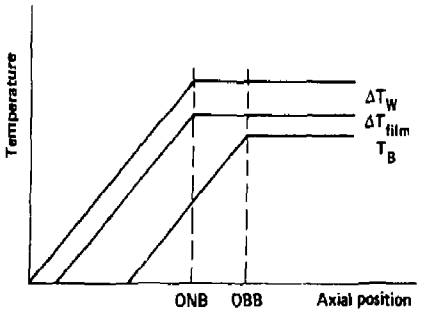

Fig. 5. Variation of temperature along the length of a water-cooled grid tube. For maximum power handling, the exit end should lie between the points ONB (onset of fully-developed subcooled nucleate boiling) and OBB (onset of bulk boiling).

make a conservative estimate of the power density limit for tubes. In Fig. 6 we have plotted the value of q that locates the point ONB at the exit end of the tube as a function of the outer diameter of the tube. For the figure we took 0.76 mm for the tube wall thickness, and we set the pressure at the exit equal to Δp, the pressure difference between entrance and exit. We have shown that 1-cm-diam tubes are allowable, and the figure shows that if tube lengths are

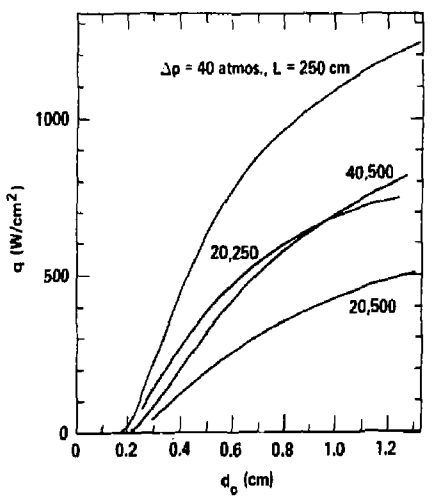

Fig. 6. The beam power density, q, that locates the axis end of a grid tube at the point ONB (Fig. 5) plotted vs d_o, the outer diameter of the tube, and the tube wall thickness was taken as 0.76 mm in each case.

less than 5 m, water cooling can increase the possible q to perhaps 700 W/cm^2, well above the 100 W/cm^2 limit for wires.

Spacings in the PDC and its Grids

All of the various spacings in the PDC are interrelated and are therefore all determined by the same considerations. The maximum separation between the plane of the suppressor grid and the adjacent ion collector is determined by the space charge of the ions in the region between the two. Space charge potential is calculated from Poisson's equation in this nearly one-dimensional geometry:

$$\frac{d^2V}{dx^2} = -\frac{\rho}{\epsilon_o} \quad ,$$

where V is the potential at position x, ρ is the charge density of the ions at position x, and ϵ_o is the permittivity of free space. The charge density, ρ, varies with x only because V does. As V increases, the ions slow down and their density increases. If some ions are reflected, their charge contributes twice to the charge density before the reflection point. Space charge potential therefore depends on the energy distribution of the incident ions and on the potentials applied to the electrodes. Numerical calculation is required to determine accurately the potential variation and therefore the largest spacings allowed before local maxima in V(x) develop.

Local maxima in potential would reflect ions that otherwise could reach the collector. Actually, no significant maxima can develop, because secondary electrons produced at the ion collector would accumulate there and cancel it out. The net effect is simply to waste the space where the potential maxima would be, since the electric field outside of the region is independent the length of that region. It is prudent, therefore, to solve Poisson's equation for the separation that locates the potential maximum at the plane of the ion collector. A smaller separation would result in an increased electric field at the grid and an increase in the capacitively stored energy.

Numerical calculations typically give a value of just over one meter for this maximum spacing in a single-stage PDC when the power density is about 100 W/cm^2 and the mean ion energy is about 150 keV. The electric field, then, is typically about 10^3 V/cm at the grid plane. At the surface of the grid elements the electric field is much higher.

The average value, E_r, of the electric field at the surface of a grid element is easily shown (using Gauss' law) to be given by

$$\bar{E}_r = \left(\frac{a}{2\pi r}\right)\left(E_1 + E_2\right) \quad ,$$

where r is the radius of the grid elements, a is

their center-to-center spacing, and E_1 and E_2 are the electric fields at some distance on either side of the grid plane. Space charge can be included to a first approximation by correcting E_1 and E_2 for space charge. Notice that $\bar{E}_T$ varies inversely with the opacity 2r/a of the grid. Typically, $\bar{E}_T \sim 10^4$ V/cm, a high but not unreasonable value.

Related to this is the question of how negative the grid potential must be to prevent electrons from leaking between wires. Figure 7 shows a plot of the potential as a function of distance normal to the grid plane. Curve a shows the potential along a line that intercepts a wire, while curve b is for a line midway between wires. Electrons with energies greater than the minimum value V_{min} midway between wires (curve b) will penetrate the grid. When electrons can be characterized by an electron temperature, T_e, the requirement is that $V_{min} \leq -3\ kT_e/e$, where k is the Boltzmann constant and e is the electronic charge. In Fig. 7 it is assumed that $T_e \sim 30$ keV. One can read from a curve like curve a in Fig. 7 the value of the negative potential required on wires of other sizes to produce the same potential distribution. The required grid voltage increases rapidly as the opacity, 2r/a, of the grid is decreased.

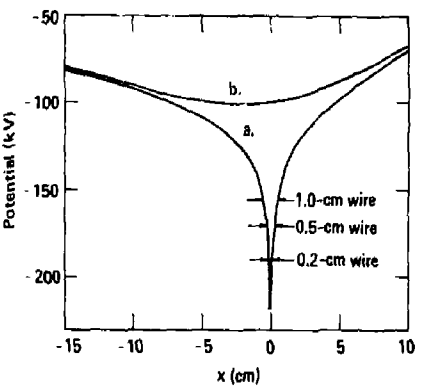

Fig. 7. The variation of potential along lines passing normally through the plane of the suppressor grid. Curve a is for a line through a grid wire, while curve b is for a line passing midway between wires. The intersection of curve a with radius of the wire shows the voltage that must be applied to produce the potential distribution shown. An electron temperature of 30 keV, which requires -100 kV for suppression, is assumed.

However, good recovery efficiency requires grids that intercept very little of the incident-ion power. The fractional power loss at the grounded grid is simply 2r/a. But, since the suppressor grid is negative and since most of the secondary electrons produced there go to the ion collector, the fractional power loss is roughly 3 x (2r/a) for that grid. Losses are discussed in more detail in Ref. 1.

It is clear that the opacity, 2r/a, of the grids is an important parameter. Efficiency demands highly transparent grids, while voltage holding considerations require that the grids be more opaque. The best compromise usually places the opacity in the range $0.0^{-} \leq 2r/a \leq 0.05$.

Reliability is improved if r and therefore a is increased, whether the grids are cooled by radiation or by convection, partly because of the reduced number of elements. But, a is restricted to $a < d/3$ (d is the separation between the grid plane and the ion collector) to limit the scattering of the ions as they pass through the grid. And, the maximum value of the effective value of d is determined by the space-charge of the ions, as it was discussed earlier. Therefore, the space-charge of the ions finally determines not only d, but a and r as well. One possibly serious consequence of this fact is that the higher limit on power density for water-cooled grids could be unavailable if the higher power density dictates that the tubes are too small to carry enough water. Since higher ion energy means lower space charge for a given power density, tandem-mirror reactors can take advantage of water cooled grids.

No mention has been made of the Debye length, which is usually an important scale length in plasmas. The Debye length can only be small compared to the grid spacings in the region before the suppressor grid. In other regions of the PDC the density of electrons is low. The Debye shielding length, λ, is given (in meters) by

$$\lambda = (7440)\ (T_e/n_e)^{1/2}\ ,$$

where T_e is the electron temperature in eV and n_e is the electron density in m^{-3}. If the density of cold electrons (created by ionization in the end tanks) is large, λ can become small in comparison with a. Then the entrance grid can become ineffective and cause the suppressor grid also to become ineffective. It is therefore necessary to limit the production rate of cold electrons in the end tanks. This imposes a limit on the gas density, which was discussed in the section on vacuum requirement.

In addition to the major dimensions just discussed, the ribbon structure of a multi-stage, Venetian-blind PDC involves many smaller details. These are treated in Ref. 13 and are not repeated here.

Vacuum Requirement

Any ion that undergoes charge exchange before it can be collected is lost from direct recovery. To reduce the loss due to this effect, the density of gas in the end tanks must be kept low. The gas density must also be kept low for other reasons. Cold electrons are produced by ionization of the background gas in the end tanks. The electrical potential in the end tanks adjusts itself until these cold electrons are lost at the same rate that they are produced. They are lost when they strike the grounded grid of the PDC. However, before being lost they may penetrate the strong magnetic field and enter the confined plasma. The cooling effect of this influx of cold electrons into the plasma and the Debye shielding length at the entrance grid must be controlled by limiting the gas density in the end tanks.

The accurate calculation of the influx of electrons and of the electron density at the grid must be done numerically for each special case, since it involves the spatial distribution of potential and of magnetic field as well as the opacity of the first PDC grid. However, we can estimate the allowed gas density in order to determine the requirements on vacuum pumping.

The current of cold electrons produced by ionization of gas in the end tanks is

$$I_e = I_i n_0 \sigma L,$$

where I_i is the current of fast ions, n_0 is the gas density, σ is the cross section for the production of free electrons by D^+ ions in D_2 gas, and L is the path length in an end tank. This establishes the vacuum requirement in the end tank imposed by the maximum allowed value of the ratio I_e/I_i, once that maximum value is established. The solid curves in Fig. 8 show the variation with ion energy of the gas pressure allowed by this effect for two possible values of the ratio I_e/I_i when $L = 15$ m.

The dashed curves in Fig. 8 show the variation of the pressure that causes a 5, 3, or 1% loss to the PDC by charge exchange. Charge exchange can occur anywhere along an ion trajectory in the end tank. Along most of the trajectory the ion energy is high. The cross section may be small, but the path length is large. Inside the PDC the ions are decelerated to lower energy where the cross section for charge exchange is large. Charge exchange in this region amounts to a reflection of the ion since the new ion, is expelled from the region of high positive potential. It is this region that causes the plateau at the right hand end of the dashed curves in Fig. 8.

Both effects, cold electron production and charge exchange loss of fast ions, cause power losses from the reactor. A compromise must be made between the cost of vacuum pumping and the value of the power saved.

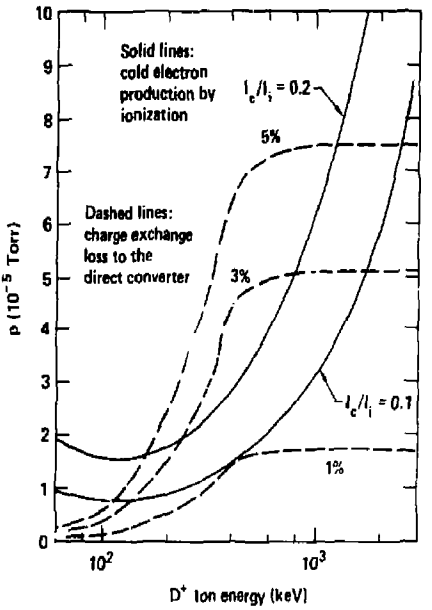

Fig. 8. The allowed gas pressure in the end tanks as a function of the mean energy of the end-loss ions. The dashed curves are determined by losses to the direct converter due to charge exchange, while the solid curves are determined by the production rate of free electrons.

The area of cryopanels needed to provide the necessary vacuum pumping is determined by the required pressure (Fig. 8) and the pumping speed of the panels. A cryopanel with two sets of chevrons has a specific pumping speed of 4.4 ℓ/s-cm^2 for a mixture of D_2 and T_2 gas when the temperature of the gas is 300 K (see Ref. 14). In Fig. 9 we have plotted the area of cryopanel required per 100 MW of ion power as a function of the ion energy in the end tanks to give the pressure shown in Fig. 8. For comparison, the surface area of the PDC is about 100 m^2 per 100 MW if radiatively cooled grids are used and possibly only 10 m^2 per 100 MW if water cooled tubes are used.

It is apparent in Fig. 9 that the required area of cryopanel is comparable to the area of the PDC, and that the cryopanel area remains nearly the same whether a PDC or a simple, thermal, plasma dump is used in the end tanks. One difference in the pumping with a PDC is that skimmers (See Fig. 10) are required to collect the cold ions that stream out along the outer magnetic field lines.

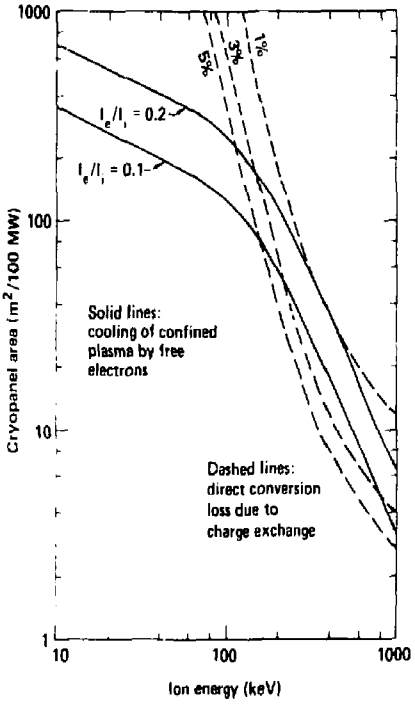

Fig. 9. The required area of cryopanels (per 100 MW of ion power into the end tanks) plotted against the mean ion energy. For comparison, about 100 m^2 or less of direct converter surface is required for 100 MW of ion power.

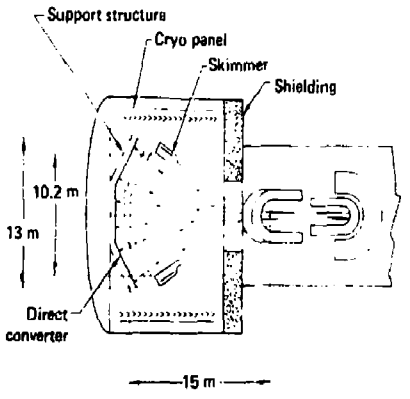

Fig. 10. The location of cryopanels and skimmers in an end tank behind neutron shielding. From Ref. 6, where 159 MW of ions with a mean energy of 395 keV were incident on the direct converter.

In either case, the cryopanels must be shielded from the fusion neutrons which otherwise would deposit an intolerable heat load on the refrigeration system.

Conclusion

The end-loss plasma from a tandem-mirror reactor, with its high minimum ion energy and the natural magnetic expansion, offers the ideal environment for direct recovery. Furthermore, the vacuum requirement is essentially unchanged by the inclusion of a plasma direct converter in the end tanks. Even the volume of the end tanks is probably unchanged, since it is determined by the cryopanels. The cryopanels must be shielded from the fusion neutrons as well as from the plasma.

Recent experimental tests of direct converters have verified many of our design concepts. However, several important points need further analysis and tests on a larger scale. Among these points is the build-up of cold plasma in the end tanks and its effect on the grids in the direct converter. Another point requiring further study is the frequency of grid failure (breaking of wires or leaking of tubes) and the consequences of grid failure. Is the rupture of a water-cooled grid catastrophic? Large scale testing at high power is required.

References

1. W. L. Barr and R. W. Moir, Lawrence Livermore National Laboratory, Report in preparation (1980).

2. W. L. Barr and R. W. Moir, paper to be presented at the 1980 Annual Meeting of the Division of Plasma Physics of the Amer. Physical Society, San Diego, California, 10-14 November 1980.

3. T. K. Fowler and B. G. Logan, Comments Plasma Phys. 2, 167 (1977).

4. G. I. Dimov, V. V. Zakaidakov, and M. E. Kishinevskiy, Fiz. Plazmy 3 (1977) 597.

5. D. E. Baldwin, B. G. Logan, and T. K. Fowler, An Improved Tandem Mirror Fusion Reactor, Lawrence Livermore National Laboratory, Livermore, California, UCID-18156 (1979).

6. G. A. Carlson et al., Tandem Mirror Reactor with Thermal Barriers, Lawrence Livermore National Laboratory, Livermore, California, UCRL-52836 (1979).

7. D. E. Baldwin, G. G. Logan, and T. C. Simonen, eds., Physics Basis for MFTF-T, Lawrence Livermore National Laboratory, Livermore, California, UCID-18496 (1980).

8. R. W. Moir and J. D. Lee, Criteria for Design of an Adiabatic Expander for a Direct Energy Converter, Lawrence Livermore National Laboratory, Livermore, California, UCRL-51351 (1973).

9. R. R. Smith, Plasma Expander for Venetian Blind Direct Converters, Lawrence Livermore National Laboratory, Livermore, California, UCRL-51371 (1973).

10. W. H. Kohl, Handbook of Materials and Techniques for Vacuum Devices (Reinhold Publishing Corp., New York, N.Y., 1967), p. 258 and Chapter 16.

11. W. D. Wood et al., Thermal Radiative Properties, (Plenum Press, 1964).

12. M. A. Hoffman, R. W. Werner, T. R. Roose, and G. A. Carlson, Nuclear Engineering and Design 36, 37-46 (1976).

13. R. W. Moir and W. L. Barr, Nucl. Fusion 13, 35 (1973).

14. T. H. Batzer, R. E. Patrick, and W. R. Call, A Neutral Beam Line Pump with Helium Cryotrapping Capability, Lawrence Livermore National Laboratory, Livermore, California, UCRL-81196 (1978).

15. G. A. Carlson, et al., Tandem Mirror Reactor with Thermal Barriers, Lawrence Livermore National Laboratory, Livermore, California, UCRL-52836 (1979).